

# Spatial Dependencies in Item Response Theory: Gaussian Process Priors for Geographic and Cognitive Measurement

Mingya Huang<sup>†</sup>Soham Ghosh<sup>\*</sup>

July 22, 2025

## Abstract

Measurement validity in Item Response Theory depends on appropriately modeling dependencies between items when these reflect meaningful theoretical structures rather than random measurement error. In ecological assessment, citizen scientists identifying species across geographic regions exhibit systematic spatial patterns in task difficulty due to environmental factors. Similarly, in Author Recognition Tests, literary knowledge organizes by genre, where familiarity with science fiction authors systematically predicts recognition of other science fiction authors. Current spatial Item Response Theory methods, represented by the 1PLUS, 2PLUS, and 3PLUS model family, address these dependencies but remain limited by (1) binary response restrictions, and (2) conditional autoregressive priors that impose rigid local correlation assumptions, preventing effective modeling of complex spatial relationships. Our proposed method, Spatial Gaussian Process Item Response Theory (SGP-IRT), addresses these limitations by replacing conditional autoregressive priors with flexible Gaussian process priors that adapt to complex dependency structures while maintaining principled uncertainty quantification. SGP-IRT accommodates polytomous responses and models spatial dependencies in both geographic and abstract cognitive spaces, where items cluster by theoretical constructs rather than physical proximity. Simulation studies demonstrate improved parameter recovery, particularly for item difficulty estimation. Empirical applications show enhanced recovery of meaningful difficulty surfaces and improved measurement precision across psychological, educational, and ecological research applications.

Keywords: Item response theory model, spatial dependency, Gaussian processes, measurement validity, latent variable modeling, large-scale data.

## 1 Introduction

Valid test construction requires understanding when item dependencies reflect meaningful structures versus measurement problems that threaten predictive accuracy. Measurement across psychology, education, and ecological assessment relies on Item Response Theory (IRT), which assumes that once we account for individual differences in underlying ability traits, test items should function independently of one another (Stout, 2002; Fox, 2010). However, violations of this local independence assumption frequently emerge in real assessment settings, creating tension between model assumptions and substantive meaning (Kang and Jeon, 2024; Brucato et al.,

---

<sup>\*</sup>University of Wisconsin–Madison

<sup>†</sup>Corresponding author. Email: mhuang233@wisc.edu

2023). Recent advances in latent space modeling have demonstrated that embedding both respondents and items in shared metric spaces can capture meaningful interactions that standard IRT models miss (Jeon et al., 2021). These violations become particularly evident in measurement contexts where spatial or contextual factors create systematic dependencies among items that reflect genuine theoretical structures rather than measurement artifacts. Such dependencies arise when items cluster not randomly, but according to meaningful organizational principles—whether geographic, cognitive, or conceptual.

## 1.1 Motivating Examples

In ecological assessment, citizen scientists identifying species from camera trap images across geographic regions show classification difficulty that varies systematically with spatial location due to environmental factors and regional expertise differences. Figure 1 illustrates this phenomenon using Serengeti camera trap data, where raw difficulty values at individual sites (left panel, computed as proportion of incorrect species identifications) show considerable spatial variation. When spatial dependencies are properly modeled, the posterior difficulty surface (right panel) reveals a coherent east-west gradient reflecting genuine ecological factors rather than random measurement error. This spatial structure demonstrates why item dependencies should not automatically be treated as measurement problems. That is, the item difficulty gradient corresponds to real environmental differences where species identification involves different cognitive demands across geographic contexts.

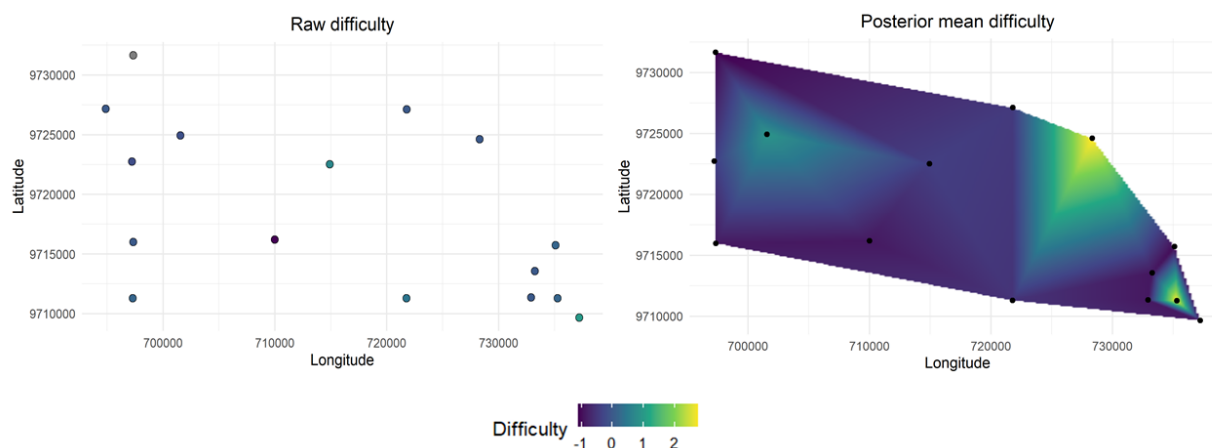


Figure 1: Spatial patterns in species identification difficulty from Serengeti camera trap data. Left panel: Raw difficulty computed as proportion of incorrect species identifications at each camera location, showing considerable spatial variation across the study region. Right panel: Posterior difficulty surface estimated using our SGP-IRT model, revealing a coherent east-west gradient that reflects genuine environmental and ecological factors rather than random measurement error. The smooth spatial structure demonstrates meaningful item dependencies that should be modeled rather than eliminated.

A parallel challenge emerges in cognitive assessment domains where items cluster by theoretical constructs rather than geographic proximity. In Author Recognition Tests, participants'

recognition patterns reveal systematic organization by literary genre—individuals who recognize science fiction authors like Ursula K. Le Guin show substantially higher recognition rates for other science fiction authors like Isaac Asimov, creating dependencies that reflect cognitive organization of literary knowledge (Stanovich and West, 1989; Moore and Gordon, 2015; Wimmer and Ferguson, 2023; Acheson et al., 2008). This recognition process involves multiple cognitive mechanisms including memory retrieval, knowledge organization by literary schemas, and confidence judgments about author familiarity, making the ART a measure of cognitive processing in the literary domain.

Both examples highlight a critical question: how should measurement models handle dependencies that carry substantive meaning while maintaining the precision and interpretability advantages of IRT approaches? The majority of current psychometric models have treated such dependencies as problems requiring correction or elimination. However, this approach may discard valuable information about construct organization, individual differences, and contextual factors that could enhance rather than compromise measurement validity.

The challenges illustrated in our motivating examples require measurement approaches that can model meaningful dependencies rather than eliminate them. While various approaches exist for handling item dependencies, the most systematic framework for spatial and contextual dependency modeling comes from spatial IRT methods that explicitly incorporate spatial structure into item parameters. The spatial IRT family, primarily represented by the 1PLUS (One-Parameter Logistic (U)sing (S)patially dependent item), 2PLUS (Two-Parameter Logistic (U)sing (S)patially dependent item), and 3PLUS (Three-Parameter Logistic (U)sing (S)patially dependent item) models (Cancado et al., 2016; Santos-Fernandez and Mengersen, 2020), provides the main approach for modeling dependencies that arise from spatial, contextual, or conceptual proximity among items. The 1PLUS model extends the Rasch model by incorporating spatial dependencies in item difficulty parameters. The 2PLUS model adds discrimination parameters that vary across spatial contexts. The 3PLUS model incorporates pseudo-guessing parameters, creating the most comprehensive spatial extension of standard IRT. However, these methods face two fundamental limitations that restrict their applicability to contemporary measurement challenges. First, they accommodate only binary responses, discarding valuable information from polytomous scales and rating formats that characterize modern assessment practice. Second, they rely on conditional autoregressive (CAR) priors that impose restrictive spatial assumptions: dependencies operate only between immediately adjacent locations, relationships are isotropic across all directions, and correlation structures cannot adapt to data patterns. These constraints prevent effective modeling of complex spatial patterns like the east-west gradient observed in our ecological example, where dependencies span long distances and vary systematically across geographic regions rather than operating only between neighboring sites.

## 1.2 Our Contributions

To address these limitations within the spatial IRT framework, we introduce a novel extension that reconceptualizes how spatial measurement models handle meaningful item dependencies. Our newly developed Spatial Gaussian Process Item Response Theory (SGP-IRT) represents a significant methodological innovation that advances beyond the 1PLUS/2PLUS/3PLUS family by treating systematic dependencies as informative structures rather than problems to eliminate, enabling enhanced measurement precision and deeper understanding of constructs and individual differences.

Our proposed method introduces four key innovations to spatial IRT methodology. First, we develop a spatial IRT extension that accommodates polytomous responses, enabling analysis of

rating scales, partial credit formats, and graded performance measures that characterize contemporary assessment across domains. Second, we introduce a novel application of flexible Gaussian process priors to replace the restrictive conditional autoregressive assumptions underlying existing spatial IRT methods, allowing data-driven learning of optimal dependency structures while maintaining uncertainty quantification. Third, we pioneer methods for extending spatial modeling beyond geographic coordinates to abstract similarity spaces derived from response patterns, enabling dependency modeling in cognitive, ecological, and other domains where items cluster by theoretical constructs rather than physical location. Fourth, we provide theoretical framework establishing the superior convergence properties of our flexible GP approach compared to the restrictive CAR priors used in 1PLUS/2PLUS/3PLUS models. Our empirical studies demonstrate improved parameter recovery and measurement precision compared to existing spatial IRT methods across diverse assessment contexts. The theoretical contributions provide principled guidance for method selection while empirical applications illustrate enhanced ability to recover meaningful difficulty surfaces and improve ability estimation precision. These innovations represent significant advances over the 1PLUS/2PLUS/3PLUS family and open new possibilities for spatial measurement applications across research domains.

The remainder of this paper reviews IRT fundamentals and existing spatial approaches, presents our proposed method, SGP-IRT, establishes new theoretical guarantees, demonstrates performance through simulation studies comparing against the spatial IRT family, and discusses implications for measurement practice across research domains.

## 2 Background

### 2.1 A brief review of Item Response Theory

Item Response Theory (IRT) provides a probabilistic framework for modeling the relationship between respondents' latent traits and their responses to test items. The theory specifies that the probability of a particular response to an item depends on both the respondent's ability level and the item's characteristics. This relationship is formalized through item response functions that map latent traits to response probabilities. The classic IRT model for dichotomous responses takes the form:

$$P(X_{ij} = 1 | \theta_i, \xi_j) = f(\theta_i; \xi_j), \quad (1)$$

where  $X_{ij}$  represents the response (0 or 1) of respondent  $i$  to item  $j$ ,  $\theta_i$  denotes the respondent's ability, and  $\xi_j$  contains the item parameters.

The Rasch model (1PL) represents the simplest IRT formulation:

$$P(X_{ij} = 1 | \theta_i, b_j) = \frac{\exp(\theta_i - b_j)}{1 + \exp(\theta_i - b_j)}, \quad (2)$$

where  $b_j$  is the item difficulty parameter. This parameter indicates the ability level at which respondents have a 0.5 probability of answering correctly. The 1PL model assumes all items have equal discrimination and no guessing.

The two-parameter logistic (2PL) model extends this framework:

$$P(X_{ij} = 1 | \theta_i, a_j, b_j) = \frac{\exp[a_j(\theta_i - b_j)]}{1 + \exp[a_j(\theta_i - b_j)]}, \quad (3)$$

where  $a_j$  represents the item discrimination parameter. This parameter governs how sharply the

probability of correct response changes with ability near the item’s difficulty point.

For items where guessing may occur (i.e., multiple choice questions), the three-parameter logistic (3PL) model adds a lower asymptote:

$$P(X_{ij} = 1|\theta_i, a_j, b_j, c_j) = c_j + (1 - c_j) \frac{\exp[a_j(\theta_i - b_j)]}{1 + \exp[a_j(\theta_i - b_j)]}, \quad (4)$$

where  $c_j$  represents the pseudo-guessing parameter. This parameter reflects the probability of correct response for respondents with extremely low ability.

## 2.2 IRT in spatial cluster detection

Recent methodological advances have extended IRT frameworks to spatial analysis problems. The approach developed by Santos-Fernandez and Mengersen (2021) reformulates spatial cluster detection as an IRT problem by conceptualizing geographic regions as “examinees” and bootstrap replications as “test items.” This innovative approach involves several key steps. First, it generates multiple bootstrap samples from the original spatial data. Then, it applies conventional cluster detection methods (such as scan statistics) to each bootstrap sample. This process produces a binary response matrix where each entry  $U_{ij}$  indicates whether region  $j$  was included in the detected cluster for replication  $i$ . Within this framework, the IRT ability parameter  $\theta_j$  represents a region’s propensity to belong to the true spatial cluster. The model estimates the probability of cluster membership using a logistic function:

$$P(U_{ij} = 1|\theta_j, a, b) = \frac{1}{1 + \exp[-a(\theta_j - b)]}. \quad (5)$$

To assess model fit, the method compares the parametric IRT model to a nonparametric estimator through an  $L^1$  distance metric:

$$T = \int_{-\infty}^{\infty} \left| \frac{1}{1 + \exp[-a(\theta - b)]} - \hat{\pi}(\theta) \right| \phi(\theta) d\theta, \quad (6)$$

where  $\hat{\pi}(\theta)$  derives from isotonic regression of the observed response proportions.

While this approach represents a significant improvement in spatial statistics, several limitations remain. First, the method’s performance depends heavily on the initial cluster detection algorithm, which may systematically miss irregularly shaped clusters. Second, the framework lacks formal statistical tests for evaluating secondary clusters. Third, while the method identifies regions with high estimated probabilities outside the primary cluster, it provides no systematic approach for investigating these regions. These limitations motivate our proposed methodological improvements.

## 3 Our Proposed Method

To overcome the limitations of existing approaches, we develop a more flexible framework that combines the strengths of IRT with Gaussian processes for spatial modeling. Our method addresses the challenges of irregular cluster shapes and provides a more systematic approach to uncertainty quantification.

**Gaussian process (GP) priors.** The core of our proposed solution is the Gaussian process, a powerful tool for modeling spatial relationships. A Gaussian process is a collection of random variables  $\{f(\mathbf{s}) : \mathbf{s} \in \mathcal{S}\}$  such that every finite vector,  $\mathbf{f} = (f(\mathbf{s}_1), \dots, f(\mathbf{s}_m))^\top$  is multivariate normal  $\mathcal{MVN}(\boldsymbol{\mu}, \boldsymbol{\Sigma})$  (Rasmussen (2004)). The mean function  $\mu(\mathbf{s}) = \mathbb{E}[f(\mathbf{s})]$  is often set to 0 for identifiability, whilst the positive-definite kernel  $k(\mathbf{s}, \mathbf{s}') = \text{cov}\{f(\mathbf{s}), f(\mathbf{s}')\}$  encodes prior beliefs about smoothness, periodicity or anisotropy. GPs deliver closed-form marginalisation, hence easy Bayesian inference; automatic uncertainty quantification through the posterior predictive variance; and universal function approximation when combined with flexible kernels (Neal, 2000).

To formalize our model, we denote the number of respondents as  $I$ , the number of items as  $J$ , and the number of response categories as  $C \geq 2$ . For each observation  $n = 1, \dots, N$  ( $N = IJ$ ) we store:

$$Y_n \in \{1, \dots, C\}, \quad i(n) \in \{1, \dots, I\}, \quad j(n) \in \{1, \dots, J\}, \quad \mathbf{x}_n \in \mathbb{R}^p.$$

When geographic coordinates are unavailable, we obtain  $\mathbf{s}_j \in \mathbb{R}^D$  ( $D = 2$  in our application in ART data) by applying a dimensionality-reduction technique such as t-SNE (van der Maaten and Hinton, 2008) or Principal Component Analysis (PCA; see Maćkiewicz and Ratajczak (1993); Greenacre et al. (2022) for comprehensive reviews) to the item-by-item similarity matrix;  $\mathbf{s}_j$  thus acts as a *latent* location for item  $j$ . In our model, each respondent has an ability  $\theta_i$ , and each item has a slope  $\alpha_j > 0$  and a vector of category difficulties  $\boldsymbol{\beta}_j = (\beta_{j1}, \dots, \beta_{jC})^\top$ . For response  $n$  the linear predictor for category  $c$  is

$$\eta_{nc} = \theta_{i(n)} - \beta_{j(n)c} + \alpha_{j(n)} \mathbf{x}_n^\top \boldsymbol{\gamma},$$

and the probability mass function is

$$\mathbb{P}(Y_n = c) = \frac{\exp(\eta_{nc})}{\sum_{k=1}^C \exp(\eta_{nk})}.$$

A key innovation in our approach is how we handle item difficulties. Items close in  $\mathbf{s}$ -space are expected to have similar difficulties. To share information effectively, we place an anisotropic squared-exponential GP prior on each category vector  $\boldsymbol{\beta}_c$ :

$$\boldsymbol{\beta}_c \sim \mathcal{N}\left(\mathbf{0}, \sigma_{\text{gp}}^2 \mathbf{K} + \sigma_{\text{nug}}^2 \mathbf{I}\right), \quad K_{jj'} = \exp\left(-\frac{1}{2} \sum_{d=1}^D \frac{(s_{jd} - s_{j'd})^2}{\ell_d^2}\right),$$

where  $\boldsymbol{\ell} = (\ell_1, \dots, \ell_D)^\top$  allows dimension-specific length-scales and  $\sigma_{\text{nug}}$  absorbs residual item-specific noise. Unlike the isotropic squared-exponential kernel  $k(\mathbf{s}, \mathbf{s}') = \sigma^2 \exp(-\|\mathbf{s} - \mathbf{s}'\|^2 / 2\ell^2)$  that assumes the same correlation length  $\ell$  in every dimension, our approach recognizes that latent maps produced by t-SNE often contain one highly-informative axis and one axis of lesser importance. Allowing individual length-scales  $\boldsymbol{\ell} = (\ell_1, \dots, \ell_D)$ —the *automatic relevance determination* kernel of MacKay (1996) – lets the data learn which directions matter, increases predictive power (Rasmussen (2004)), and facilitates interpretability through the relative magnitudes of  $\ell_d$  (Durrande et al. (2011)). For numerical stability and to maintain the prior centered at  $\mathbf{0}$ , we parameterize

$$\boldsymbol{\beta}_c = \sigma_{\text{gp}} \mathbf{L}_K \mathbf{z}_c, \quad \mathbf{z}_c \sim \mathcal{N}(\mathbf{0}, \mathbf{I}),$$

where  $\mathbf{L}_K \mathbf{L}_K^\top = \mathbf{K}$ .

For the remaining parameters, we set the priors

$$\theta_i \sim \mathcal{N}(0, \sigma_\theta^2), \quad \alpha_j = 1 + \tilde{\alpha}_j, \quad \tilde{\alpha}_j \sim \mathcal{N}(0, \sigma_\alpha^2),$$

$$\sigma_\theta, \sigma_\alpha, \sigma_{gp}, \ell_d, \sigma_{mug} \sim \text{HalfNormal}(0, 1).$$

A soft sum-to-zero constraint is imposed on every  $\beta_c$  to fix location, which is a common assumption in many item–response models – parameters are only identified up to an additive constant ( $\theta_i + c$ ,  $\beta_{jc} + c$  is observationally equivalent) (Fox, 2010).

**Implementation details** Our model is implemented in `Stan`, leveraging its efficient Bayesian inference capabilities. Posterior sampling uses the No-U-Turn Hamiltonian Monte-Carlo (NUTS) algorithm (Hoffman and Gelman (2011)) with `adapt_delta = 0.99`, which indicates the target acceptance-probability that NUTS tries to achieve during the adaptation phase when it tunes the leap-frog step size. Additionally, we choose `max_treedepth = 15`, which is an upper bound on the depth of the binary tree that NUTS builds while it doubles the trajectory length. We ensure convergence by examining trace plots, confirming  $\hat{R} < 1.01$  (Vehtari et al. (2021)), and checking effective sample sizes.

**Distinction from the 3PLUS model.** To clarify the contributions of our approach, it is important to distinguish it from the citizen-science implementation 3PLUS of Santos-Fernandez and Mengersen (2021). While both methods leverage IRT principles, they differ in several key aspects. The 3PLUS model was designed for camera-trap accuracy data in which (i) the responses are strictly *binary* (correct/incorrect) and (ii) each observation is indexed by a physical site and a biological species. Its spatial layer is therefore either a first–order conditional–autoregressive (CAR) prior (see Besag et al. (1991)) on a Voronoi adjacency graph or a stationary covariance that depends on great-circle distance.

In contrast, our framework offers several advantages: it permits an arbitrary number of categories through the soft-max likelihood; places a Gaussian process prior on the vector of item difficulties, which yields a smooth global correlation surface rather than purely local CAR smoothing; and allows the coordinates  $s_j$  to be either genuine longitude/latitude or latent positions extracted from item similarity. As a consequence, our model can be applied to rating-scale data, partial-credit items, or any test where a latent geometry is more natural than a geographic one. Methodologically, 3PLUS decomposes difficulty into *site* and *species* effects and offers on/off switches for guessing ( $c$ ) and item slopes through its 1PL/2PL/3PL variants, whereas our specification retains a single spatially–smoothed difficulty surface and an item-specific slope but does not include a guessing parameter by default. From an inferential perspective, we use weak half-normal priors that shrink scale parameters toward zero, whereas 3PLUS employs wide Uniform/Gamma priors to remain diffuse.

## 4 Theoretical Guarantees

In our model, each item  $j$  is assigned a difficulty surface  $f_c(s_j) = \beta_{jc}$  for a response category  $c$ . When the number of respondents  $I$  is large, the binary likelihood may be second-order expanded around the truth; conditional on the high-dimensional ability vector, the posterior for each difficulty surface behaves like non-parametric regression with Gaussian noise. In that regard, we first

write down the linear predictor for respondent  $i$  on item  $j$  as

$$\eta_{ij}(\beta_{jc}) = \theta_i + \alpha_j \mathbf{x}_{ij}^\top \gamma - \beta_{jc}.$$

For brevity, we call  $h_{ij} := \theta_i + \alpha_j \mathbf{x}_{ij}^\top \gamma$ . Since  $Y_{ij} | h_{ij}, \beta_{jc} \sim \text{Bern}(\pi_{ij})$  with  $\pi_{ij} = \sigma(h_{ij} - \beta_{jc})$  and  $\sigma(\cdot)$  being the sigmoid function, for a single item  $j$ , the conditional log-likelihood as a function of  $\beta_{jc}$  is

$$l_j(\beta_{jc}) = \sum_{i=1}^I \{Y_{ij}[h_{ij} - \beta_{jc}] - \log(1 + \exp(h_{ij} - \beta_{jc}))\} \quad (7)$$

Throughout this section, we fix the respondent abilities  $\theta_i$  and the nuisance parameters  $(\alpha_j, \gamma)$  - they will be estimated jointly in the full Bayesian analysis, but for studying the marginal posterior of the difficulty surface these quantities may be regarded as conditioning variables. We denote their true values by  $(\theta_i^0, \alpha_j^0, \gamma^0)$  and write  $h_{ij}^0 := \theta_i^0 + \alpha_j^0 \mathbf{x}_{ij}^\top \gamma^0$ . Taylor-expanding 7 around the truth  $\beta_{jc}^0$ :

$$l_j(\beta_{jc}) = l_j(\beta_{jc}^0) + (\beta_{jc} - \beta_{jc}^0) l_j'(\beta_{jc}^0) + \frac{1}{2} (\beta_{jc} - \beta_{jc}^0)^2 l_j''(\tilde{\beta}_{jc})$$

where  $\tilde{\beta}_{jc} \in (\beta_{jc}, \beta_{jc}^0)$ . Conditional on the fixed abilities  $\{\theta_i^0\}$ , the summands  $Y_{ij} - \pi_{ij}^0$  with  $\pi_{ij}^0 = \sigma(h_{ij}^0 - \beta_{jc}^0)$  are independent, mean-zero and have finite variance  $\pi_{ij}^0(1 - \pi_{ij}^0)$ . Therefore, the Lindeberg-Feller Central Limit Theorem gives

$$I^{-1/2} l_j'(\beta_{jc}^0) \implies \mathcal{N}(0, \tilde{w}_j), \quad \text{as } I \rightarrow \infty.$$

with  $\tilde{w}_j = I^{-1} \sum_{i=1}^I \pi_{ij}^0(1 - \pi_{ij}^0)$ . In addition,  $I^{-1} l_j''(\tilde{\beta}_{jc}) \rightarrow -\tilde{w}_j$  uniformly on a neighbourhood of  $\beta_{jc}^0$  by the Law of Large Numbers. Hence with probability  $1 - o(1)$ , we have the second-order local asymptotic normality expansion,

$$l_j(\beta_{jc}) - l_j(\beta_{jc}^0) = -\frac{I \tilde{w}_j}{2} (\beta_{jc} - \beta_{jc}^0 - \xi_j)^2 + \mathcal{O}_p(1), \quad (8)$$

where  $\xi_j = I^{-1} l_j'(\beta_{jc}^0) / I \tilde{w}_j$  satisfies  $\xi_j \xrightarrow{d} \mathcal{N}(0, (I \tilde{w}_j)^{-1})$ . Exponentiating 8 shows that, conditional on the latent abilities, the likelihood for  $\beta_{jc}$  is locally equivalent to

$$\tilde{L}_j(\beta_{jc}) = \exp \left\{ -\frac{I \tilde{w}_j}{2} (\beta_{jc} - y_{jc})^2 \right\}, \quad y_{jc} = \beta_{jc}^0 + \xi_j \stackrel{\text{iid}}{\sim} \mathcal{N}(\beta_{jc}^0, (I \tilde{w}_j)^{-1})$$

Thus, posterior inference for the vector  $\beta_{\cdot c}$  is first-order asymptotically equivalent to non-parametric Gaussian regression on the lattice of item locations

$$y_{jc} = f_0(\mathbf{s}_j) + \epsilon_{jc}, \quad \epsilon_{jc} \stackrel{\text{iid}}{\sim} \mathcal{N}(0, \sigma^2/I), \quad (9)$$

with  $f_0(\mathbf{s}_j) = \beta_{jc}^0$ . Hence all asymptotic questions about recovering  $\beta_{\cdot c}$  may be addressed with the vast existing literature on Bayesian non-parametric Gaussian regression ([van der Vaart and van Zanten, 2008](#); [Ghosal and van der Vaart, 2007](#)). In this reduced problem our model places an anisotropic squared-exponential Gaussian process prior on  $f_0$ , whereas the 3PLUS family endows  $f_0$  with an intrinsic first-order conditional autoregressive (CAR) prior. The two priors encode very different smoothness assumptions: the squared-exponential GP supports functions that are infinitely differentiable, while the intrinsic first-order CAR corresponds to a Sobolev space of

smoothness  $m = 1$ . In order to assess the posterior contraction rates to the true difficulty surface  $f_0$  for each of the anisotropic GP and the CAR priors, we state the following theoretical results.

### Assumptions and notations

(A1) Items sit on a regular  $m \times \dots \times m$  ( $m^D = J$ ) grid with spacing  $h = m^{-1}$ .

(A2) The unknown surface  $f_0$  belongs to the Hölder ball  $\mathcal{C}^\nu(B)$ , with  $\nu > 1$ :

$$\mathcal{C}^\nu(B) = \{f : |\partial^\alpha f(\mathbf{s}) - \partial^\alpha f(\mathbf{t})| \leq B \|\mathbf{s} - \mathbf{t}\|^{\nu - |\alpha|}, 0 \leq |\alpha| < \nu\}.$$

(A3) The anisotropic GP prior has mean 0; and kernel  $k(\mathbf{s}, \mathbf{t}) = \sigma_{\text{gp}}^2 \exp[-\frac{1}{2}(\mathbf{s} - \mathbf{t})^\top \Lambda^{-1}(\mathbf{s} - \mathbf{t})]$  with  $\Lambda = \text{diag}(\lambda_1^2, \dots, \lambda_D^2)$ .

(A4) Intrinsic first-order CAR with precision  $\tau(D - \rho W)$  and  $\rho \in (0, 1)$ :

$$\beta_{\cdot c} \mid \tau, \rho \sim \mathcal{N}_J(\mathbf{0}, [\tau(D - \rho W)]^{-1}),$$

where  $W = (w_{j,j'})_{1 \leq j, j' \leq J}$ , each element  $w_{j,j'} = \mathbb{1}\{\mathbf{s}_j \text{ and } \mathbf{s}_{j'} \text{ are nearest-neighbours}\}$  and  $D = \text{diag}(d_1, \dots, d_J)$  with  $d_j = \sum_{j'} w_{j,j'}$ .

We denote the posterior mean under the GP prior as  $\hat{f}_{\text{GP}}$  and the posterior mean under the CAR prior as  $\hat{f}_{\text{CAR}}$ . Assumption (A1) reflects technical convenience – a regular  $m^D$  lattice makes the pairwise spacing  $h \approx J^{-1/D}$  explicit. Letting  $J \rightarrow \infty$  amounts to observing the difficulty surface on an increasingly fine, deterministic design. Irregular designs introduce additional random-design terms that obscure the comparison between priors.

**Theorem 1.** *Under the assumptions (A1), (A2) and the anisotropic GP prior in assumption (A3), for a sufficiently large constant  $M > 0$ ,*

$$\Pi_{P_{f_0}}(\|f - f_0\|_{L^2} > M\epsilon_J \mid \mathbf{y}) \rightarrow 0$$

where  $\epsilon_J = J^{-\nu/(2\nu+D)}$ .

The proof of Theorem 1 follows the posterior contraction results of Ghosal et al. (2000, Theorem 2.1) and van der Vaart and van Zanten (2011). Specifically, we need to show a KL-neighborhood condition, which ensures the GP posterior can concentrate near  $f_0$ , followed by a sieve entropy condition, which effectively keeps the parameter space finite-dimensional at the target resolution  $\epsilon_J$ . Finally, we want to guarantee a prior mass condition which guarantees the posterior cannot put appreciable mass on functions further than  $M\epsilon_J$  from  $f_0$ . Now, we study the minimax lower bound for the CAR posterior mean.

To establish these conditions rigorously, we leverage the Reproducing Kernel Hilbert Space (RKHS) associated with our Gaussian process prior, which encapsulates the smoothness properties imposed by our GP prior through its anisotropic squared-exponential kernel (Wahba, 1990; van der Vaart and van Zanten, 2009). Characterizing the support of the GP prior in terms of its RKHS is essential to verifying the prior mass condition. Indeed, the RKHS norm directly quantifies smoothness assumptions, enabling precise specification of prior concentration rates around functions in Hölder or Sobolev classes (van der Vaart and van Zanten, 2008, 2011).

**Theorem 2.** For every  $\nu > 1$ ,

$$\inf_{\hat{f}} \sup_{f_0 \in \mathcal{C}^\nu(B)} \mathbb{E} \|\hat{f} - f_0\|_{L^2}^2 \gtrsim J^{-2/(2+D)}$$

In particular,  $\mathbb{E} \|\hat{f}_{\text{CAR}} - f_0\|_{L^2}^2 = \mathcal{O}(J^{-2/(2+D)})$ .

Theorem 2 gives a minimax benchmark for recovering the latent difficulty surface  $f_0$  under assumptions (A1) and (A2) in the sense that, the rate  $J^{-2/(2+D)} = m^{-2}$  is the information-theoretic optimum for this design. In particular, even though the Hölder exponent  $\nu$  could be large, the lattice design saturates the rate at  $2/(2+D)$ ; smoother truth cannot be exploited without a denser grid. We show the minimaxity by invoking a Fourier-based Le Cam’s two-point method (Tsybakov, 2009, Chapter 2). First, two Fourier “spikes” are used to establish a minimax *lower* bound via Le Cam’s two-point lemma (Lemmas 8–9). Secondly, Proposition 10 shows that because the intrinsic CAR prior and the Gaussian likelihood are both diagonal in the same Fourier basis, the posterior mean is an explicit linear shrinker whose bias and variance can be summed frequency-by-frequency. Tuning the global precision  $\tau$  at order  $m^2$  balances the two contributions and achieves the very same rate, proving that the CAR posterior mean is minimax-optimal. Discrete Fourier techniques identical to ours have been used in functional linear regression – for instance Cai and Hall (2006) (functional PCA regression) and Yuan and Cai (2010) use eigen-basis constructions to derive minimax lower bounds for estimating functional coefficients, the core idea being the same: treat the hardest to estimate eigenfunction as a Fourier-like basis element and apply a two-hypothesis or Fano’s argument.

Thus, combining the findings from the aforementioned Theorems 1 and 2, we have that the anisotropic GP prior dominates CAR for smooth surfaces.

**Corollary 3.** Under the assumptions (A1)–(A4), we have

$$\frac{\mathbb{E}_{f_0} \|\hat{f}_{\text{GP}} - f_0\|_{L^2}^2}{\mathbb{E}_{f_0} \|\hat{f}_{\text{CAR}} - f_0\|_{L^2}^2} \rightarrow 0,$$

as  $J \rightarrow \infty$ .

**Asymptotic dominance.** For sufficiently many items, Corollary 3 suggests that the GP will uniformly outperform CAR in recovering the latent difficulty landscape. The result reflects the GP prior’s ability to adapt to unknown smoothness and anisotropy through its length-scale matrix  $\Lambda$ , whereas the CAR prior imposes a fixed, low-order Markov random-field roughness penalty. When the true surface is smoother than first-order differences can capture, the GP borrows strength over larger neighbourhoods and therefore enjoys substantially lower estimation error.

## 5 Simulation Study

We designed a simulation study to assess the performance of our spatial multinomial item response model. The simulation reflects a typical IRT setting with spatially referenced items and includes a single covariate effect, similar to Santos-Fernandez and Mengersen (2021). To facilitate direct comparison with contemporary IRT models, we focus on the binary response case (i.e., two response categories) and generate data using a softmax formulation.

**Simulation setup** Our simulation includes 200 individuals, each representing a respondent whose latent ability is to be estimated. These respondents interact with 50 spatially located items. To incorporate item-specific features, we generate a single covariate from a uniform distribution over  $[-1, 1]$ , which could represent characteristics such as image quality in Santos-Fernandez and Mengersen (2021). Each item is assigned spatial coordinates (e.g., representing longitude and latitude), drawn independently from a uniform distribution over the unit interval.

Additionally, to capture item-level grouping effects that often occur in real-world settings, we assign each item  $j$  to one of  $S = 5$  latent categories (e.g., species), sampled uniformly. These category labels enable us to study subgroup heterogeneity in item difficulty or covariate interactions, reflecting the complexity often found in practical applications.

For the parameter values driving this simulation, we set each individual’s ability to be drawn from a normal distribution with  $\sigma_\theta^{\text{true}} = 1$ . The discrimination parameter for item  $j \in \{1, 2, \dots, 50\}$  is generated with  $\sigma_\alpha^{\text{true}} = 0.5$ . For each response category  $c \in \{1, 2\}$ , the item difficulties are modeled as a spatial process following the approach described in our proposed methods. The true hyperparameters for the exponential kernel  $\mathbf{K}$  are set as  $\sigma_{gp}^{\text{true}} = 1.0$  (for the GP marginal variance),  $l^{\text{true}} = 0.3$  (lengthscale), and  $\sigma_{nug}^{\text{true}} = 0.1$  (nugget variance). This configuration yields a total of  $N = 200 \times 50 = 10,000$  observations for our analysis.

**Simulation results** For clarity in the following comparisons, we refer to our proposed method as SGP-IRT (Spatial Gaussian Process - Item Response Theory). We first compare the parameter estimation accuracy across different models. Figure 2 presents the Root Mean Squared Errors (RMSEs) of the posterior-estimated parameters  $\theta$ ,  $\alpha$  and  $\beta$  (for Category 2, as Category 1 is taken to be the reference level) as well as the corresponding variance parameters  $\sigma_\theta$  and  $\sigma_\alpha$ . These metrics are computed with respect to the true parameter values specified previously. We compare our SGP-IRT with three established methods: 1PLUS, 2PLUS, and 3PLUS.

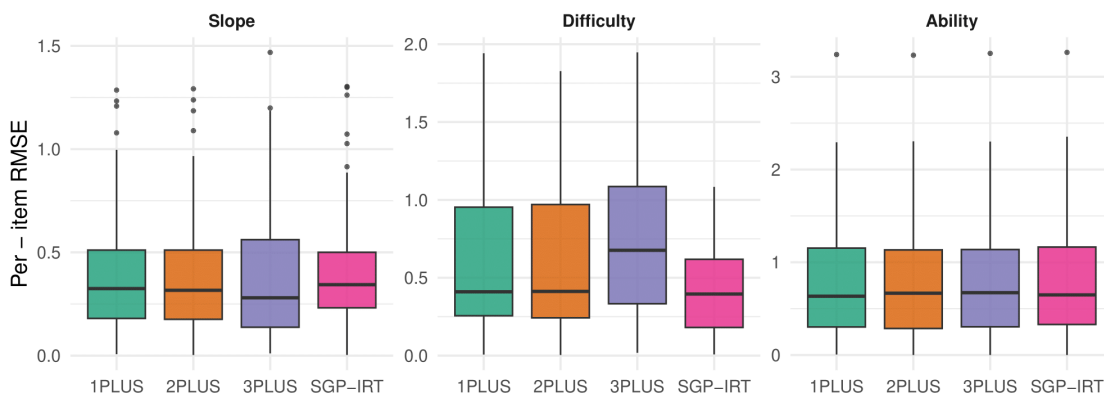


Figure 2: Parameter estimation accuracy comparison across four spatial IRT methods. Box plots show Root Mean Squared Errors (RMSE) for posterior-estimated parameters  $\theta$  (ability),  $\alpha$  (discrimination), and  $\beta$  (difficulty for Category 2, with Category 1 as reference), as well as variance parameters  $\sigma_\theta$  and  $\sigma_\alpha$ . Results are based on 200 respondents and 50 spatially located items. SGP-IRT demonstrates better performance, particularly for difficulty parameter estimation (mean RMSE of 0.201 vs. 0.709 for 2PLUS), reflecting the effectiveness of Gaussian process spatial smoothing in borrowing information across spatially proximate items.

Figure 2 highlights the better performance of SGP-IRT across all the methods. Examining these results in detail, we find that all four methods perform comparably in estimating respondent

ability ( $\theta$ ), with minimal differences in RMSE values. For item discrimination,  $\text{SGP-IRT}$  slightly outperforms the others with the lowest RMSE, indicating better recovery of the slope parameter  $\alpha$ . The most striking advantage of our approach appears in the estimation of the difficulty parameter  $\beta$ , where  $\text{SGP-IRT}$  achieves a mean RMSE of 0.201, substantially lower than the next best performer ( $\text{2PLUS}$  at 0.709). This dramatic improvement reflects the key strength of GP-based spatial smoothing, which effectively borrows information across items using their spatial proximity. The  $\text{3PLUS}$  model shows notably inferior performance here, likely due to limitations of the CAR structure in capturing complex spatial variation compared to the flexibility offered by Gaussian processes. Furthermore,  $\text{SGP-IRT}$  estimates both variance components ( $\sigma_\theta$  and  $\sigma_\alpha$ ) much more accurately than other methods. The RMSEs drop from approximately 0.9 in classical models to 0.132 and 0.053 respectively, confirming that the hierarchical GP structure substantially improves hyperparameter recovery. These results collectively demonstrate the parameter estimation advantages of our approach.

**Remark.** Note that our simulation uses  $\nu \approx 2$  (twice differentiable GP draw),  $D = 2$ . Plugging it into the rates from Corollary 3 gives  $J^{-2/3}$  for GP and  $J^{-1/2}$  for CAR. That would imply that the ratio of the MSEs should be  $\asymp J^{-1/6}$ . With  $J = 50$ , this predicts an approximately 35% reduction in RMSE. The observed empirical improvement is substantially greater, with the GP-based RMSE being over four times smaller than the CAR-based one.

**Multinomial response data** To demonstrate our model’s ability to handle multinomial response data (more than two categories), we extend the same spatial-softmax simulation described previously from  $C = 2$  to  $C = 4$  outcome categories. Specifically, we draw true category- $c$  difficulties  $\beta_{jc}$  jointly from a 4D Gaussian process with the same specifications as in the original setting. Then for each observation  $n$  we build the 4-vector of logits  $\eta_{nc}$ , apply the softmax to obtain  $\mathbb{P}(Y_n = c)$ , and sample  $Y_n \in \{1, 2, 3, 4\}$ . Finally, we fit our model and compute, for each category  $c$ , the RMSE of the posterior mean  $\hat{\beta}_{jc}$  over the 50 items.

Figure 3 shows that our  $\text{SGP-IRT}$  recovers category-specific difficulty surfaces with modest spread and no obvious degradation as  $C$  increases. Categories 1 and 4, which in our simulation were assigned somewhat smoother GP surfaces, exhibit the lowest median RMSE (around 0.8 and 0.7, respectively), while category 3, whose true  $\beta_{\cdot,3}$  surface was effectively rougher, shows a slightly larger median RMSE. Overall, these results confirm that our approach scales naturally to multinomial outcomes and that the GP prior continues to provide good recovery even when there are more than two response categories.

**Predictive performance** Beyond parameter recovery, we are interested in how well each fitted model translates its latent parameter estimates into concrete predictions. To assess this, we compute posterior-predictive classification accuracy using a decision-theoretic framework. For every observation  $n$  in the simulated data, we first obtain its posterior predictive probability of falling in the positive class (here, Category 2). Specifically, for each MCMC draw corresponding to the species  $s = 1, 2, \dots, 5$ , we evaluate  $\eta_n^{(s)} = \text{logit}^{-1} \left( \theta_{i(n)}^{(s)} - \beta_{j(n),2}^{(s)} + \alpha_{j(n)}^{(s)} x_n \right)$ , which represents the success-probability implied by sample  $s$  for respondent  $i(n)$  answering item  $j(n)$  with covariate value  $x_n$ . We then average over the posterior draws to obtain the posterior mean predictive probability  $\hat{\eta}_n = \sum_{s=1}^5 \eta_n^{(s)} / 5$ . Thereafter, we classify the response as positive whenever  $\hat{\eta}_n > 0.5$ . Comparing these binary predictions with the true labels yields the *highest* overall accuracy for  $\text{SGP-IRT}$  (**0.688**), with  $\text{3PLUS}$  (0.669) as a close second, followed by  $\text{2PLUS}$  (0.665) and  $\text{1PLUS}$  (0.661). This approach properly accounts for parameter uncertainty by using the posterior expectation  $\hat{\eta}_n$  rather than relying on a single point estimate. To provide a more comprehensive evaluation of predic-

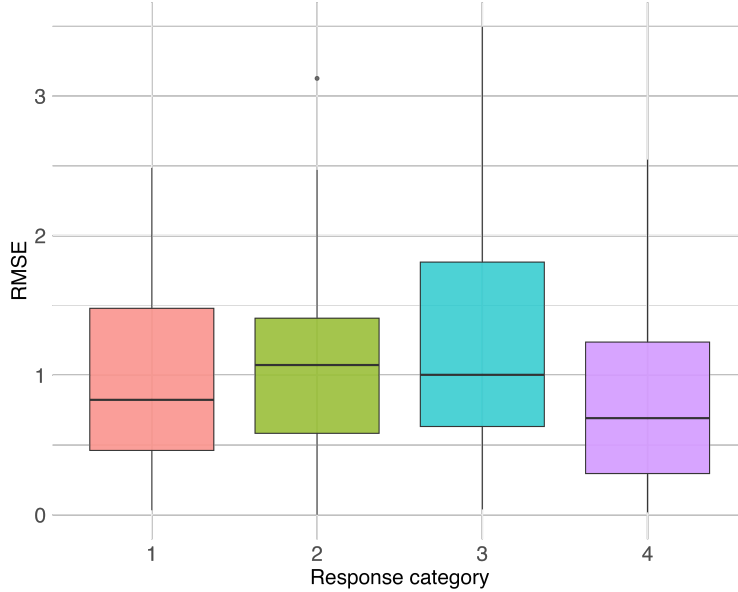


Figure 3: Recovery performance for multinomial response data with four outcome categories. Box plots show item-level RMSE for posterior mean difficulty estimates  $\hat{\beta}_{jc}$  across 50 items for each response category  $c \in \{1, 2, 3, 4\}$ . Categories 1 and 4, assigned smoother Gaussian process surfaces in simulation, exhibit lower median RMSE, while Category 3, with a rougher true surface, shows slightly higher RMSE. Results demonstrate that SGP-IRT scales naturally to polytomous outcomes without performance degradation.

tive performance beyond a single threshold, we also compute Receiver Operating Characteristic (ROC) curves for each method. These curves, shown in Figure 4, are generated by sweeping the classification threshold between 0 and 1 and recording the associated true-positive and false-positive rates at each point. The resulting area under the curve (AUC) provides a threshold-free summary of each model’s discriminative power. In terms of AUC, SGP-IRT again achieves the highest value (**0.74**), compared to 0.7182 for 3PLUS, 0.7137 for 2PLUS, and 0.71 for 1PLUS. This consistent pattern across both classification accuracy and AUC metrics confirms the better predictive performance of our proposed method.

## 6 Empirical Study

### 6.1 Author Recognition Test (ART) Data

In this empirical study, we applied the SGP-IRT framework to a dataset derived from an Author Recognition Test administered to older adults (Wimmer and Ferguson, 2023). ART responses typically reveal latent patterns of participant knowledge and preference, particularly when authors share genre similarities or reader exposure profiles, reflecting underlying cognitive organization of literary knowledge (Moore and Gordon, 2015; Stanovich and West, 1989). However, standard IRT methods treat items independently, ignoring the underlying relationships or similarity between authors that might influence participants’ recognition (explored in detail by McGeown et al. (2020) for instance). To address this limitation, we begin by exploring the underlying structure of the ART items. We hypothesize that authors belonging to the same genre are not independent entities; rather, they share latent attributes that lead to correlated recognition patterns among respondents. By integrating latent spatial structure through a t-SNE embedding and a Gaussian Process

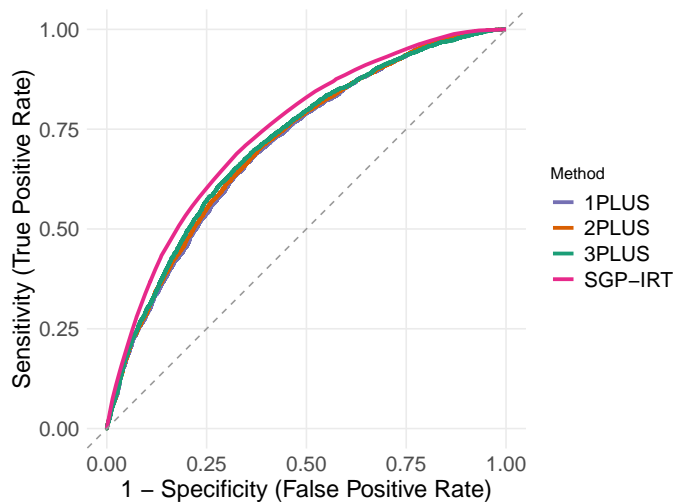


Figure 4: Receiver Operating Characteristic (ROC) curves comparing predictive performance across four spatial IRT methods. Curves are generated by sweeping classification thresholds between 0 and 1 and recording true-positive and false-positive rates for binary classification tasks. The consistent pattern across both classification accuracy and AUC metrics confirms better predictive performance of the proposed method, properly accounting for parameter uncertainty through posterior expectation rather than point estimates.

prior, we successfully captured the patterns of item difficulty and response similarity across three distinct literary genres: `SciFiFantasy`, `SocialPoliticalCommentary`, and `Suspense`. Our approach illuminated genre-specific response behaviors and provided intuitive visualizations of item difficulties and genre-level operating characteristics. Furthermore, by incorporating respondents’ vocabulary scores as a grouping covariate, our `SGP-IRT` model improved in richness and predictive power, demonstrating enhanced performance in out-of-sample prediction for two of the three genres analyzed.

Our dataset comprises responses from older adults (aged approximately 50–80 years, with a total sample size of 321 respondents) who completed various measures of print exposure. We focus on three subsets of the Author Recognition Test (ART): `SciFiFantasy` (25 items), `SocialPoliticalCommentary` (10 items), and `Suspense` (25 items). Each item captures a binary response (0/1), indicating recognition of an author as a genuine fiction writer. During preprocessing, we converted responses to numeric format, removed missing values, and excluded items with zero variance.

### 6.1.1 Spatial Structure of Item Difficulty

Assuming a latent spatial structure that reflects underlying similarities among items, we now examine how this structure informs the estimation of item difficulty parameters through our Gaussian Process prior. This approach allows us to leverage the spatial relationships between items to better understand the difficulty variability across genres.

Figure 5 displays each item positioned according to its t-SNE coordinates, with color indicating the posterior mean of its difficulty and shape indicating the genre membership. This visualization serves both as a diagnostic of model fit and as a practical map for item selection and interpretation across genres. Items located near each other in t-SNE space share similar response profiles, while their colors reveal whether they are relatively easy (negative difficulty, shown in purple) or hard (positive difficulty, shown in yellow). In simpler terms, items that respondents tend to treat simi-

larly are pulled close together in the visualization; items answered very differently are pushed far apart.

The most striking finding is that item difficulty is not random; rather, it forms a continuous landscape. The easiest items (darkest purple) cluster in the centre-left region – predominantly mid-ranking *SciFiFantasy* items along with a few *Suspense* items. In contrast, the hardest items (bright yellow) appear in two distinct areas: along the upper-left rim of the *Suspense* cluster and on the far right where many *SocialPoliticalCommentary* items are located. These yellow areas represent authors who are rarely recognized by participants. Importantly, the color field changes smoothly over the 2-D manifold, precisely the behavior that our anisotropic squared exponential GP prior is designed to capture. This smooth transition in difficulty levels across the spatial map validates our modeling approach and provides a visually intuitive representation of how item difficulty varies across the latent space.

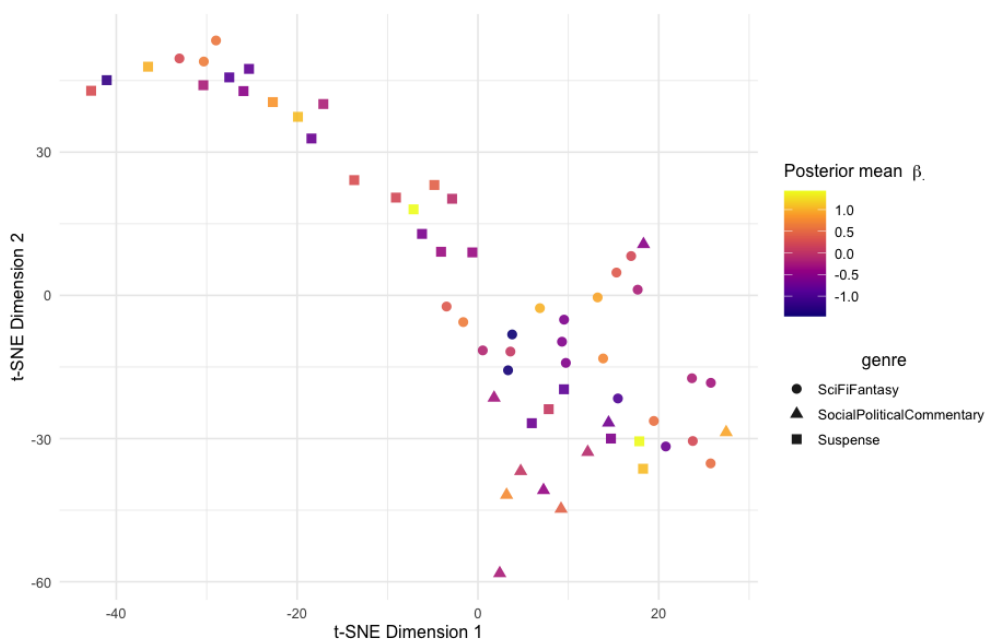


Figure 5: Posterior mean item difficulty across literary genres in t-SNE coordinate space. Each point represents an author item positioned according to t-SNE coordinates derived from response similarity patterns, with color indicating posterior mean difficulty and shape indicating genre membership. This figure tells that item difficulty forms a continuous landscape rather than random variation, with easiest items clustering in the center-left region and hardest items appearing along distinct boundaries. The smooth color transitions validate our anisotropic Gaussian process prior design for capturing spatial dependency structures.

### 6.1.2 Genre-level operating characteristics

Moving beyond individual items, we now analyze how each genre functions as a whole in measuring participants’ recognition abilities. The Item Characteristic Curve (ICC) provides essential information about item behavior across different ability levels. These curves, calculated using  $\bar{P}_g(\theta) = J_g^{-1} \sum_{j \in g} \mathbb{P}(Y_{ij} = 1 \mid \theta, j \in g)$ , with  $J_g$  being the number of items related to the genre  $g$ , show the probability of a positive response as a function of the latent trait ( $\theta$ ). Higher curves indicate items that are easier to endorse and are more likely to be recognized by individuals with lower ability levels.

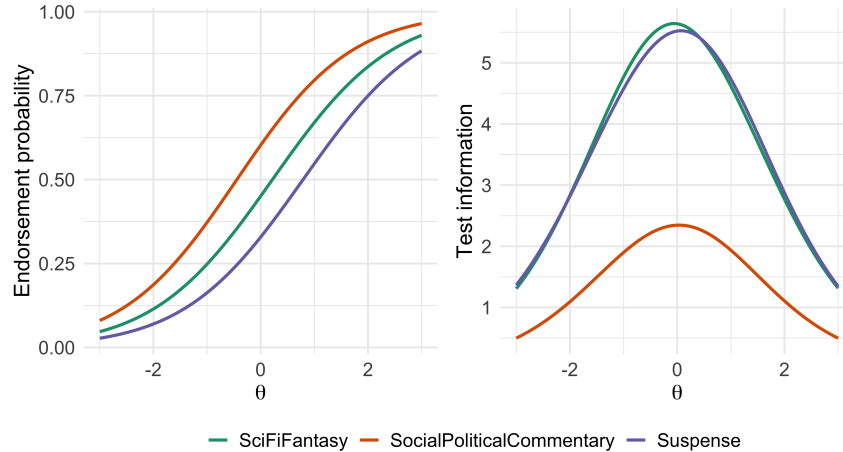


Figure 6: Average endorsement-probability and total information curves. Higher curves in the left panel indicate easier items; steeper slopes indicate greater discrimination. Taller peaks in the right panel imply lower posterior s.e. in  $\theta$  estimation near that ability level.

The left panel of Figure 6 reveals distinct patterns across the three genres.

The `SocialPoliticalCommentary` items are easiest overall, while `Suspense` items are the most difficult. The `SciFiFantasy` genre occupies an intermediate position between these extremes. The roughly parallel slopes observed for `SciFiFantasy` and `Suspense` indicate comparable discrimination power, whereas the upward shift of the `SocialPoliticalCommentary` curve reflects uniformly lower difficulty but not necessarily greater information content.

To complement these findings and gain deeper insight into each genre’s measurement precision, we examine Total Information Curves (TICs). These curves show how much information a test provides ( $\mathcal{I}$ ) about a person’s ability at different points along the ability continuum, and are created by summing the individual item information curves for all items in each genre. The right panel of Figure 6 also displays these information functions, highlighting important differences between genres. Both `SciFiFantasy` and `Suspense` reach similar peaks near  $\mathcal{I} \approx 5.4$  at  $\theta = 0$  (corresponding to a posterior standard error of  $\approx 0.43$ ), and maintain substantial information content ( $\mathcal{I} > 2$ ) across a wide ability range ( $|\theta| \approx 2$ ). In contrast, `SocialPoliticalCommentary` peaks at only  $\mathcal{I} \approx 2.4$  (standard error  $\approx 0.64$ ), offering substantially less precision across the ability spectrum. These findings have direct implications for test design and administration – for maximally efficient measurement, especially in adaptive testing contexts, we understand that `SciFiFantasy` and `Suspense` items should be prioritized early in the assessment process, with `SocialPoliticalCommentary` items reserved primarily for fine-tuning once the participant’s ability level ( $\theta$ ) has been approximately located.

### 6.1.3 Out-of-Sample Prediction Analysis

We assessed the out-of-sample predictive accuracy of the competing IRT methods using Leave-One-Out Cross-Validation (LOOCV) along with the Watanabe-Akaike Information Criterion (WAIC). LOOCV evaluates model performance by iteratively omitting each observation, fitting the model to the remaining data, and then assessing how accurately the fitted model predicts the omitted observation. We efficiently approximated these predictive distributions using Pareto-smoothed importance sampling (PSIS) (Vehtari et al., 2024). Table 1 summarizes the LOO Information Criterion (LOOIC) and WAIC metrics, both quantifying predictive performance, with lower values

indicating better out-of-sample predictive accuracy. The bold-faced entries in Table 1 highlight the improved predictive performance within each genre. For `SciFiFantasy`, `SGP-IRT` achieves the best predictive fit with the smallest LOOIC (4680.7) and WAIC (4675.3), demonstrating its robustness in capturing the latent spatial structure of author recognition. In the `SocialPoliticalCommentary` genre, `2PLUS` attains the best predictive accuracy (LOOIC = 2338.0, WAIC = 2322.6), slightly outperforming `SGP-IRT`. Interestingly, for `Suspense`, `SGP-IRT` outperforms all competing methods (LOOIC = 6349.4, WAIC = 6345.7), highlighting the model’s capacity to flexibly adapt to the latent difficulty surfaces across items.

The observed variation in predictive performance across genres aligns with underlying differences in item difficulty structures. Specifically, the improved predictive performance of `SGP-IRT` in `SciFiFantasy` and `Suspense` underscores its effectiveness in modeling smoothly varying latent difficulty surfaces informed by the t-SNE embedding. In contrast, the slightly improved performance of `2PLUS` for `SocialPoliticalCommentary` suggests that in contexts with simpler spatial dependence structures, simpler models might achieve similar predictive accuracy without requiring complex Gaussian-process smoothing.

Table 1: Predictive performance comparison using Leave-One-Out Cross-Validation (LOOCV) and Watanabe-Akaike Information Criterion (WAIC) across three literary genres. Lower values indicate superior out-of-sample predictive accuracy. Bold entries highlight best performance within each genre.

Genre	Method	LOOIC	WAIC
SciFiFantasy	1PLUS	4788.2	4781.6
	2PLUS	4698.7	4688.6
	3PLUS	4686.9	4679.5
	<b>SGP-IRT</b>	<b>4680.7</b>	<b>4675.3</b>
SocialPoliticalCommentary	1PLUS	2405.3	2399.9
	<b>2PLUS</b>	<b>2338.0</b>	<b>2322.6</b>
	3PLUS	2352.5	2343.5
	SGP-IRT	2343.5	2335.2
Suspense	1PLUS	6451.4	6446.9
	2PLUS	6389.2	6381.5
	3PLUS	6371.2	6364.2
	<b>SGP-IRT</b>	<b>6349.4</b>	<b>6345.7</b>

## 7 Discussion

This study introduces a Gaussian process extension to IRT models that addresses two fundamental limitations in spatial modeling of discrete response data: the restriction to binary outcomes and the inflexibility of conditional autoregressive priors. Our theoretical and empirical results demonstrate that `SGP-IRT` provides improved parameter recovery and maintains competitive predictive performance across diverse applications, from ecological citizen science to psychometric assessment.

The theoretical foundation established through Theorems 1 and 2 reveals a trade-off in spatial smoothing approaches. While CAR priors impose first-order Markov constraints that limit their ability to capture long-range dependencies, Gaussian processes with squared-exponential kernels can adapt to unknown smoothness levels and exploit spatial correlations at multiple scales.

The convergence rate advantage of GP priors becomes increasingly important as datasets grow larger—a particularly relevant finding given the expanding scale of modern survey and citizen science initiatives. The anisotropic kernel specification offers practical advantages beyond theoretical optimality, allowing the model to discover and exploit asymmetries in latent spatial dimensions without requiring domain-specific tuning.

Our methodological innovations extend beyond theoretical improvements to address practical measurement challenges. The extension to polytomous responses enables modeling of rich categorical data structures that are increasingly common in practical applications. More significantly, our use of latent spatial coordinates derived from response similarity matrices fundamentally expands the scope of spatial IRT beyond geographical applications. This innovation enables spatial modeling in abstract spaces where traditional coordinate systems are unavailable, as demonstrated in our Author Recognition Test analysis where genre-based spatial structures emerge naturally from response patterns. The empirical results illuminate important performance boundaries that guide practical model selection. *SGP-IRT*'s advantage in parameter recovery reflects its ability to borrow strength across spatially proximate items, particularly beneficial when individual items receive sparse observations. However, these gains come with computational considerations that practitioners must weigh. The Stan implementation leverages efficient Hamiltonian Monte Carlo sampling, though costs scale cubically with spatial locations due to covariance matrix operations.

Several extensions merit future investigation, including incorporating temporal dynamics for longitudinal applications, developing non-stationary covariance functions for domains with varying correlation structures, and exploring alternative dimensionality reduction techniques beyond t-SNE. The framework also suggests natural extensions to network-structured data and hierarchical spatial models that accommodate multiple scales of dependence.

## 8 Acknowledgment

We would like to express our sincere appreciation to Dr. Daniel Bolt for his insightful discussion and invaluable suggestions, which have been crucial in shaping the direction and improving the quality of this study. We also appreciate the Center for High Throughput Computing (CHTC) in the Department of Computer Science at UW-Madison for their technical support in this research ([Center for High Throughput Computing, 2006](#)).

## References

- Acheson, D. J., Wells, J. B., and MacDonald, M. C. (2008). New and updated tests of print exposure and reading abilities in college students. *Behavior Research Methods*, 40(1):278–289.
- Besag, J., York, J., and Mollié, A. (1991). Bayesian image restoration, with two applications in spatial statistics. *Annals of the Institute of Statistical Mathematics*, 43(1):1–20.
- Brucato, M., Frick, A., Pichelmann, S., Nazareth, A., and Newcombe, N. S. (2023). Measuring spatial perspective taking: Analysis of four measures using item response theory. *Topics in Cognitive Science*, 15(1):46–74.
- Cai, T. T. and Hall, P. (2006). Prediction in functional linear regression. *The Annals of Statistics*, 34(5):2159 – 2179.

- Cancado, A. L. F., Gomes, A. E., da Silva, C. Q., Oliveira, F. L. P., and Duczmal, L. H. (2016). An item response theory approach to spatial cluster estimation and visualization. *Environmental and Ecological Statistics*, 23(3):435–451.
- Center for High Throughput Computing (2006). Center for High Throughput Computing.
- Durrande, N., Ginsbourger, D., Roustant, O., and Carraro, L. (2011). Additive covariance kernels for high-dimensional gaussian process modeling. *Annales de la faculté des sciences de Toulouse Mathématiques*, 21.
- Fox, J.-P. (2010). *Estimation of Bayesian Item Response Models*, pages 67–106. Springer New York, New York, NY.
- Ghosal, S., Ghosh, J. K., and van der Vaart, A. W. (2000). Convergence rates of posterior distributions. *The Annals of Statistics*, 28(2):500–531.
- Ghosal, S. and van der Vaart, A. (2007). Convergence rates of posterior distributions for noniid observations. *The Annals of Statistics*, 35(1).
- Greenacre, M., Groenen, P. J. F., Hastie, T., D’Enza, A. I., Markos, A., and Tuzhilina, E. (2022). Principal component analysis. *Nature Reviews Methods Primers*, 2(1):100.
- Hoffman, M. D. and Gelman, A. (2011). The no-u-turn sampler: Adaptively setting path lengths in hamiltonian monte carlo.
- Jeon, M., Jin, I. H., Schweinberger, M., and Baugh, S. (2021). Mapping unobserved item–respondent interactions: A latent space item response model with interaction map. *Psychometrika*, 86(2):378–403.
- Kammann, E. E. and Wand, M. P. (2003). Geoadditive models. *Journal of the Royal Statistical Society. Series C (Applied Statistics)*, 52(1):1–18.
- Kang, I. and Jeon, M. (2024). A recent development of a network approach to assessment data: Latent space item response modeling for intelligence studies. *Journal of Intelligence*, 12(4).
- Lindgren, F., Rue, H., and Lindström, J. (2011). An explicit link between gaussian fields and gaussian markov random fields: the stochastic partial differential equation approach. *Journal of the Royal Statistical Society: Series B (Statistical Methodology)*, 73(4):423–498.
- MacKay, D. J. C. (1996). *Bayesian Non-Linear Modeling for the Prediction Competition*, pages 221–234. Springer Netherlands, Dordrecht.
- Maćkiewicz, A. and Ratajczak, W. (1993). Principal components analysis (pca). *Computers & Geosciences*, 19(3):303–342.
- McGeown, S., Bonsall, J., Andries, V., Howarth, D., and Wilkinson, K. (2020). Understanding reading motivation across different text types: qualitative insights from children. *Journal of Research in Reading*, 43(4):597–608.
- Moore, M. and Gordon, P. C. (2015). Reading ability and print exposure: item response theory analysis of the author recognition test. *Behavior Research Methods*, 47(4):1095–1109.
- Neal, R. (2000). Monte carlo implementation of gaussian process models for bayesian regression and classification.

- Rasmussen, C. E. (2004). *Gaussian Processes in Machine Learning*, pages 63–71. Springer Berlin Heidelberg, Berlin, Heidelberg.
- Rue, H. and Held, L. (2005). *Gaussian Markov Random Fields: Theory And Applications (Monographs on Statistics and Applied Probability)*. Chapman & Hall/CRC.
- Santos-Fernandez, E. and Mengersen, K. (2020). Bayesian item response models for citizen science ecological data. *arXiv preprint arXiv:2003.06966*.
- Santos-Fernandez, E. and Mengersen, K. (2021). Understanding the reliability of citizen science observational data using item response models. *Methods in Ecology and Evolution*, 12(8):1533–1548.
- Stanovich, K. E. and West, R. F. (1989). Exposure to print and orthographic processing. *Reading Research Quarterly*, 24(4):402–433.
- Stout, W. (2002). Psychometrics: From practice to theory and back. *Psychometrika*, 67:485–518.
- Tsybakov, A. B. (2009). *Lower bounds on the minimax risk*, pages 77–135. Springer New York, New York, NY.
- van der Maaten, L. and Hinton, G. (2008). Visualizing data using t-sne. *Journal of Machine Learning Research*, 9(86):2579–2605.
- van der Vaart, A. and van Zanten, H. (2011). Information rates of nonparametric gaussian process methods. *Journal of Machine Learning Research*, 12(60):2095–2119.
- van der Vaart, A. W. and van Zanten, J. H. (2008). Rates of contraction of posterior distributions based on gaussian process priors. *The Annals of Statistics*, 36(3).
- van der Vaart, A. W. and van Zanten, J. H. (2009). Adaptive Bayesian estimation using a Gaussian random field with inverse Gamma bandwidth. *The Annals of Statistics*, 37(5B):2655 – 2675.
- Vehtari, A., Gelman, A., Simpson, D., Carpenter, B., and Bürkner, P.-C. (2021). Rank-Normalization, Folding, and Localization: An Improved  $\hat{R}$  for Assessing Convergence of MCMC (with Discussion). *Bayesian Analysis*, 16(2).
- Vehtari, A., Simpson, D., Gelman, A., Yao, Y., and Gabry, J. (2024). Pareto smoothed importance sampling. *Journal of Machine Learning Research*, 25(72):1–58.
- Wahba, G. (1990). *Spline Models for Observational Data*. CBMS-NSF Regional Conference Series in Applied Mathematics. Society for Industrial and Applied Mathematics.
- Wimmer, L. and Ferguson, H. J. (2023). Testing the validity of a self-report scale, author recognition test, and book counting as measures of lifetime exposure to print fiction. *Behavior Research Methods*, 55(1):103–134.
- Yuan, M. and Cai, T. T. (2010). A reproducing kernel hilbert space approach to functional linear regression. *The Annals of Statistics*, 38(6).

## A Proofs

We present the proofs of our theoretical results in this section.

## A.1 Proof of Theorem 1

We prove the result in five steps. We start by proving the following auxiliary lemmas and then stitch them together via the general posterior-contraction theorem of [Ghosal et al. \(2000\)](#).

### A.1.1 Auxiliary lemmas

**Lemma 4** (Metric entropy of the RKHS unit ball). *Let  $\mathbb{H}_1 = \{f \in \mathcal{H}_k : \|f\|_{\mathcal{H}_k} \leq 1\}$  be the unit ball in the RKHS of the anisotropic squared-exponential kernel  $k$  in (A3). For every fixed  $\nu > 0$*

$$\log N(\delta, \mathbb{H}_1, \|\cdot\|_{\infty}) \leq C_{\nu} \delta^{-D/\nu}, \quad 0 < \delta < \frac{1}{2}.$$

*Proof.* We follow a detailed Fourier-truncation construction that appears in [van der Vaart and Zanten \(2011, Sect. 3.2\)](#). We work on the torus  $\mathbb{T}^D = [0, 1]^D$  and write  $e_{\boldsymbol{\kappa}}(\mathbf{s}) = e^{2\pi i \langle \boldsymbol{\kappa}, \mathbf{s} \rangle}$  for  $\boldsymbol{\kappa} \in \mathbb{Z}^D$ . The squared-exponential kernel admits the Fourier expansion

$$k(\mathbf{s}, \mathbf{t}) = \sum_{\boldsymbol{\kappa} \in \mathbb{Z}^D} \lambda_{\boldsymbol{\kappa}} e_{\boldsymbol{\kappa}}(\mathbf{s}) \overline{e_{\boldsymbol{\kappa}}(\mathbf{t})}, \quad \lambda_{\boldsymbol{\kappa}} = \sigma_{\text{gp}}^2 \prod_{d=1}^D \lambda_d (2\pi)^{-D/2} \exp(-2\pi^2 \langle \boldsymbol{\kappa}, \boldsymbol{\Lambda} \boldsymbol{\kappa} \rangle).$$

Hence every  $f \in \mathcal{H}_k$  has Fourier coefficients  $(c_{\boldsymbol{\kappa}})_{\boldsymbol{\kappa} \in \mathbb{Z}^D}$  that satisfy

$$f = \sum_{\boldsymbol{\kappa}} c_{\boldsymbol{\kappa}} e_{\boldsymbol{\kappa}}, \quad \|f\|_{\mathcal{H}_k}^2 = \sum_{\boldsymbol{\kappa}} \frac{|c_{\boldsymbol{\kappa}}|^2}{\lambda_{\boldsymbol{\kappa}}} \leq 1. \quad (10)$$

Because  $\lambda_{\boldsymbol{\kappa}}$  is strictly positive, this implies

$$|c_{\boldsymbol{\kappa}}| \leq \lambda_{\boldsymbol{\kappa}}^{1/2} = C_0 \exp(-\alpha \|\boldsymbol{\kappa}\|^2), \quad C_0 = \sigma_{\text{gp}} \left( \prod_d \lambda_d (2\pi)^{-D/2} \right)^{1/2}, \quad \alpha = \pi^2 \min_d \lambda_d^{-1} > 0. \quad (11)$$

Fix  $\delta \in (0, \frac{1}{2})$  and choose the truncation level

$$K(\delta) := \left\lceil \sqrt{\frac{1}{\alpha} \log(C_1/\delta)} \right\rceil, \quad C_1 := 4C_0 \sum_{\boldsymbol{\kappa} \in \mathbb{Z}^D} e^{-\alpha \|\boldsymbol{\kappa}\|^2} < \infty. \quad (12)$$

Split  $f = f_K + r_K$  where  $f_K = \sum_{\|\boldsymbol{\kappa}\|_{\infty} \leq K(\delta)} c_{\boldsymbol{\kappa}} e_{\boldsymbol{\kappa}}$ . The remainder term is bounded in the sup-norm by

$$\|r_K\|_{\infty} \leq \sum_{\|\boldsymbol{\kappa}\|_{\infty} > K(\delta)} |c_{\boldsymbol{\kappa}}| \leq C_0 \sum_{\|\boldsymbol{\kappa}\|_{\infty} > K(\delta)} e^{-\alpha \|\boldsymbol{\kappa}\|^2} \leq \delta/2, \quad (13)$$

by our choice of  $K(\delta)$ . Let  $\mathcal{F}_K = \{f_K : f \in \mathbb{H}_1\}$  be the set of truncated functions. The number of retained Fourier modes is  $m := (2K(\delta) + 1)^D = \mathcal{O}((\log(1/\delta))^{D/2})$ . For any  $f_K \in \mathcal{F}_K$ , we can

bound its sup-norm using the Cauchy-Schwarz inequality:

$$\begin{aligned}
\|f_K\|_\infty &\leq \sum_{\|\kappa\|_\infty \leq K(\delta)} |c_\kappa| = \sum_{\|\kappa\|_\infty \leq K(\delta)} \frac{|c_\kappa|}{\sqrt{\lambda_\kappa}} \sqrt{\lambda_\kappa} \\
&\leq \left( \sum_{\|\kappa\|_\infty \leq K(\delta)} \frac{|c_\kappa|^2}{\lambda_\kappa} \right)^{1/2} \left( \sum_{\|\kappa\|_\infty \leq K(\delta)} \lambda_\kappa \right)^{1/2} \\
&\leq \|f\|_{\mathcal{H}_k} \left( \sum_{\kappa \in \mathbb{Z}^D} \lambda_\kappa \right)^{1/2} \leq M,
\end{aligned}$$

for some constant  $M$  since the sum of eigenvalues is finite for the squared-exponential kernel. The set  $\mathcal{F}_K$  is a subset of an  $m$ -dimensional vector space where all elements are uniformly bounded by  $M$ . A standard result for the metric entropy of a bounded set in a finite-dimensional space gives

$$\log N(\delta/2, \mathcal{F}_K, \|\cdot\|_\infty) \leq m \log \left( \frac{4M}{\delta} \right) \lesssim \left( \log \frac{1}{\delta} \right)^{D/2} \log \frac{1}{\delta} = \left( \log \frac{1}{\delta} \right)^{D/2+1}.$$

Since any function  $f \in \mathbb{H}_1$  can be approximated by some  $f_K \in \mathcal{F}_K$  within  $\delta/2$ , a  $\delta/2$ -cover for  $\mathcal{F}_K$  serves as a  $\delta$ -cover for  $\mathbb{H}_1$ . Thus,

$$\log N(\delta, \mathbb{H}_1, \|\cdot\|_\infty) \leq \log N(\delta/2, \mathcal{F}_K, \|\cdot\|_\infty) \lesssim \left( \log \frac{1}{\delta} \right)^{D/2+1}.$$

Because  $(\log(1/\delta))^p = o(\delta^{-q})$  as  $\delta \downarrow 0$  for any  $p, q > 0$ , we may bound the polylogarithmic term by a polynomial one:  $(\log(1/\delta))^{D/2+1} \leq C_\nu \delta^{-D/\nu}$  for every fixed  $\nu > 0$  once  $\delta$  is sufficiently small, which establishes the bound.  $\square$

**Lemma 5 (KL mass).** *For every  $0 < \varepsilon < 1/2$  let  $\mathcal{K}_J(\varepsilon) = \{f : \text{KL}(\mathbb{P}_{f_0}^J, \mathbb{P}_f^J) < J\varepsilon^2\}$ . Then*

$$\Pi(\mathcal{K}_J(\varepsilon)) \geq \exp(-C J\varepsilon^2).$$

*Proof.* Under the working model  $y_j = f(\mathbf{s}_j) + \varepsilon_j$ ,  $\varepsilon_j \stackrel{\text{i.i.d.}}{\sim} \mathcal{N}(0, \sigma^2/I)$ , the Kullback–Leibler distance between  $\mathbb{P}_{f_0}^J$  and  $\mathbb{P}_f^J$  is

$$\text{KL}(\mathbb{P}_{f_0}^J, \mathbb{P}_f^J) = \frac{IJ}{2\sigma^2} \|f - f_0\|_J^2 \leq \frac{IJ}{2\sigma^2} \|f - f_0\|_2^2, \quad (14)$$

where the last inequality uses  $\|g\|_J \leq \|g\|_2$  on the unit cube. Now, we fix the constant  $c_0 := \sqrt{\frac{2\sigma^2}{I}}$ . Then from Equation 14,  $\|f - f_0\|_2 < c_0 \varepsilon \implies \text{KL}(\mathbb{P}_{f_0}^J, \mathbb{P}_f^J) < J\varepsilon^2$ . Hence

$$B_2(f_0, c_0 \varepsilon) \subseteq \mathcal{K}_J(\varepsilon), \quad B_2(f_0, r) := \{f : \|f - f_0\|_2 < r\}. \quad (15)$$

Using Lemma 3 in [van der Vaart and van Zanten \(2011\)](#), there exists  $C_1 > 0$  such that for every  $r \in (0, \frac{1}{2})$ ,

$$\Pi(B_2(f_0, r)) \geq \exp(-C_1 r^{-D/\nu}). \quad (16)$$

Take  $r = c_0\varepsilon$  in (16) and combine with (15):

$$-\log \Pi(\mathcal{K}_J(\varepsilon)) \leq C_1(c_0\varepsilon)^{-D/\nu}.$$

Now compare the exponents  $J\varepsilon^2$  and  $\varepsilon^{-D/\nu}$ . Because  $\varepsilon_J^{2+D/\nu} = J^{-1}$ , for every  $\varepsilon \geq \varepsilon_J$  one has  $\varepsilon^{-D/\nu} \leq J\varepsilon^2$ . Therefore choosing  $C := C_1c_0^{-D/\nu}$  gives

$$-\log \Pi(\mathcal{K}_J(\varepsilon)) \leq C J\varepsilon^2,$$

which is exactly the bound in Lemma 5. The inequality is trivial for  $\varepsilon \geq \frac{1}{2}$  because the KL neighbourhood has probability 1.  $\square$

**Lemma 6** (existence of exponentially powerful tests). *For any  $r > 0$  there exists a measurable function  $\phi_J : \mathbb{R}^J \rightarrow \{0, 1\}$  such that*

$$\mathbb{P}_{f_0}^J(\phi_J = 1) + \sup_{\|f - f_0\|_J \geq 2r} \mathbb{P}_f^J(\phi_J = 0) \leq \exp(-c I J r^2).$$

*Proof.* The proof proceeds by constructing an explicit test  $\phi_J$  and separately bounding its Type-I and Type-II error probabilities.

**Test Definition.** Define the test statistic as the sum of squared residuals relative to  $f_0$ :

$$T_J := \sum_{j=1}^J \{y_j - f_0(\mathbf{s}_j)\}^2.$$

We will reject the null hypothesis  $H_0 : f = f_0$  if  $T_J$  is too large. Let  $x = \frac{IJr^2}{8\sigma^2}$ . We define a deviation term based on the Laurent-Massart concentration inequality:

$$D(J, r) := \frac{\sigma^2}{I} \left( 2\sqrt{Jx} + 2x \right) = \frac{\sigma^2}{I} \left( 2\sqrt{J \frac{IJr^2}{8\sigma^2}} + 2 \frac{IJr^2}{8\sigma^2} \right) = Jr\sigma\sqrt{\frac{I}{2}} + \frac{IJr^2}{4}.$$

We set the rejection region  $\mathcal{R}$  using this deviation:

$$\mathcal{R} := \left\{ T_J > \frac{J\sigma^2}{I} + D(J, r) \right\}, \quad \text{and let } \phi_J = \mathbf{1}_{\mathcal{R}}.$$

**Type-I Error Bound.** Under the null hypothesis  $H_0 : f = f_0$ , we have  $y_j - f_0(\mathbf{s}_j) = \varepsilon_j$  where  $\varepsilon_j \sim \mathcal{N}(0, \sigma^2/I)$ . Let  $Z_j := I\varepsilon_j^2/\sigma^2 \sim \chi_1^2$ , so that their sum  $Z := \sum_{j=1}^J Z_j \sim \chi_J^2$ . The test statistic can be written as  $T_J = \frac{\sigma^2}{I}Z$ . The probability of a Type-I error is:

$$\mathbb{P}_{f_0}^J(\phi_J = 1) = \mathbb{P} \left( \frac{\sigma^2}{I}Z > \frac{J\sigma^2}{I} + D(J, r) \right) = \mathbb{P} \left( Z - J > \frac{I}{\sigma^2}D(J, r) \right).$$

By our definition of  $D(J, r)$ , the deviation is exactly  $2\sqrt{Jx} + 2x$ . We can now directly apply the Laurent-Massart inequality ( $\mathbb{P}(Z - J \geq 2\sqrt{Jx} + 2x) \leq e^{-x}$ ):

$$\begin{aligned}\mathbb{P}_{f_0}^J(\phi_J = 1) &\leq \exp(-x) \\ &= \exp\left(-\frac{IJr^2}{8\sigma^2}\right).\end{aligned}$$

This bounds the Type-I error as required.

**Type-II Error Bound.** Now, fix an alternative hypothesis  $H_1 : f$  such that  $\delta := \|f - f_0\|_J \geq 2r$ . Under  $H_1$ , the term  $y_j - f_0(\mathbf{s}_j) = (f(\mathbf{s}_j) - f_0(\mathbf{s}_j)) + \varepsilon_j$  is a normal variable with mean  $\mu_j = f(\mathbf{s}_j) - f_0(\mathbf{s}_j)$  and variance  $\sigma^2/I$ . Therefore, the test statistic  $T_J$  follows a scaled non-central chi-squared distribution:

$$T_J = \sum_{j=1}^J (\mu_j + \varepsilon_j)^2 \sim \frac{\sigma^2}{I} \cdot \chi_J^2(\lambda),$$

where the non-centrality parameter  $\lambda$  is given by:

$$\lambda = \frac{I}{\sigma^2} \sum_{j=1}^J \mu_j^2 = \frac{IJ\delta^2}{\sigma^2}.$$

The probability of a Type-II error is  $\mathbb{P}_f^J(\phi_J = 0) = \mathbb{P}_f^J(T_J \leq \frac{J\sigma^2}{I} + D(J, r))$ . A non-central chi-squared variable  $\chi_J^2(\lambda)$  can be approximated by a normal distribution for large  $J$  or large  $\lambda$ . Specifically,  $\frac{\chi_J^2(\lambda) - (J + \lambda)}{\sqrt{2(J + 2\lambda)}} \approx \mathcal{N}(0, 1)$ . We standardize our variable:

$$\mathbb{P}_f^J(\phi_J = 0) = \mathbb{P}\left(\frac{\chi_J^2(\lambda) - (J + \lambda)}{\sqrt{2(J + 2\lambda)}} \leq \frac{(J + \frac{I}{\sigma^2}D(J, r)) - (J + \lambda)}{\sqrt{2(J + 2\lambda)}}\right).$$

The argument of the standard normal CDF  $\Phi(\cdot)$  is  $z = \frac{\frac{I}{\sigma^2}D(J, r) - \lambda}{\sqrt{2(J + 2\lambda)}}$ . Since  $\delta \geq 2r$ , the non-centrality parameter  $\lambda$  is the dominant term, making the numerator negative. For large  $J$ , the numerator is approximately  $-\lambda$  and the denominator is approximately  $\sqrt{4\lambda}$ . A more careful calculation gives:

$$z \approx \frac{-IJ\delta^2/\sigma^2}{\sqrt{4IJ\delta^2/\sigma^2}} = \frac{-IJ\delta^2/\sigma^2}{2\delta\sqrt{IJ}/\sigma} = -\frac{\delta\sqrt{IJ}}{2\sigma}.$$

Since  $\delta \geq 2r$ , we have  $z \leq -\frac{2r\sqrt{IJ}}{2\sigma} = -\frac{r\sqrt{IJ}}{\sigma}$ . Using the standard Gaussian tail bound  $\Phi(z) \leq e^{-z^2/2}$  for  $z \leq 0$ , we get:

$$\begin{aligned}\mathbb{P}_f^J(\phi_J = 0) &\leq \exp\left(-\frac{1}{2}\left(\frac{r\sqrt{IJ}}{\sigma}\right)^2\right) \\ &= \exp\left(-\frac{IJr^2}{2\sigma^2}\right).\end{aligned}$$

Combining the two error bounds with a constant  $c = \frac{1}{8\sigma^2}$ , we have shown that for any  $r > 0$ :

$$\mathbb{P}_{f_0}^J(\phi_J = 1) + \sup_{\|f - f_0\|_J \geq 2r} \mathbb{P}_f^J(\phi_J = 0) \leq 2 \exp(-c I J r^2),$$

This proves the lemma. □

**Lemma 7** (sieve entropy and tail probability). *Define the rate  $\varepsilon_J = J^{-\nu/(2\nu+D)}$  and the sieve*

$$\mathcal{F}_J = \{f : \|f\|_{\mathcal{H}_k} \leq R_J := J^{D/(4\nu+2D)}\}.$$

For  $J$  sufficiently large

$$\log N(\varepsilon_J/\sqrt{2}, \mathcal{F}_J, \|\cdot\|_\infty) \leq C_1 J \varepsilon_J^2, \quad \Pi(\mathcal{F}_J^c) \leq \exp(-C_2 J \varepsilon_J^2).$$

*Proof.* For any semi-norm  $\|\cdot\|$ , radius  $\delta > 0$  and  $R > 0$ ,

$$N(\delta, R\mathbb{H}_1, \|\cdot\|) = N\left(\frac{\delta}{R}, \mathbb{H}_1, \|\cdot\|\right), \quad (17)$$

because  $\|Rf - Rg\| = R\|f - g\|$ . Now, for the squared-exponential kernel,

$$\log N(\delta, \mathbb{H}_1, \|\cdot\|_\infty) \leq C_* (\log \frac{1}{\delta})^{\frac{D}{2}+1}, \quad 0 < \delta < \frac{1}{2}, \quad (18)$$

(van der Vaart and van Zanten, 2011, Lemma 6). Put  $\delta_J = \varepsilon_J/\sqrt{2}$  and  $\tilde{\delta}_J = \delta_J/R_J$ . Then

$$\log N(\delta_J, \mathcal{F}_J, \|\cdot\|_\infty) \leq C_* \left(\log \frac{1}{\delta_J}\right)^{\frac{D}{2}+1}.$$

Because  $\log \frac{1}{\delta_J} = \frac{1}{2} \log J$ , the RHS is  $\mathcal{O}((\log J)^{\frac{D}{2}+1})$ . Since  $J \varepsilon_J^2 = J^{D/(2\nu+D)}$  grows like a power of  $J$ , for large  $J$   $(\log J)^{\frac{D}{2}+1} = o(J \varepsilon_J^2)$ , which yields the desired entropy bound with a suitable  $C_1$ .

The prior tail bound can be provided using the following set of arguments.

By the Borell–Sudakov–Tsirelson inequality for a centred Gaussian measure on  $\mathcal{H}_k$ ,

$$\Pi(\|f\|_{\mathcal{H}_k} > R) \leq \exp(-R^2/2), \quad R > 0.$$

Taking  $R = R_J$  gives

$$-\log \Pi(\mathcal{F}_J^c) \geq \frac{1}{2} R_J^2 = \frac{1}{2} J^{D/(2\nu+D)} = \frac{1}{2} J \varepsilon_J^2,$$

so the claim holds with  $C_2 = 1/2$ . □

*Proof of Theorem 1.* With Lemmas 4–7 we verify the three conditions of Ghosal et al. (2000, Thm. 2.1):

The prior mass condition is verified using Lemma 5 with  $\varepsilon = \varepsilon_J/\sqrt{2}$ . The existence of an exponentially powerful test is done using Lemma 6 with  $r = M\varepsilon_J$  and  $M > 0$  large enough. Finally, the entropy and tail probability bounds are provided in Lemma 7.

Hence there exists  $M > 0$  such that

$$\Pi(\|f - f_0\|_2 > M\varepsilon_J \mid y_{1:J}) \xrightarrow{\mathbb{P}_{f_0}} 0.$$

Because  $\|g\|_2 \leq \|g\|_\infty$  on  $[0, 1]^D$ , the above implies the  $L^2$  statement in Theorem 1. □

## A.2 Proof of Theorem 2

We keep the regression reduction  $y_j = f_0(\mathbf{s}_j) + \varepsilon_j$ ,  $\varepsilon_j \stackrel{\text{i.i.d.}}{\sim} \mathcal{N}(0, \sigma^2/I)$ , on the regular  $m^D = J$  lattice of Assumption (A1). The first half of the proof of Theorem 2 uses Le Cam's two-point method to establish the fastest possible convergence rate any estimator can achieve for this problem. The second half, i.e., Proposition 10 proves that the CAR posterior mean can actually achieve this rate. We start by proving the two auxiliary ingredients, Lemma 8 and Lemma 9 to establish the minimax lower bound.

**Lemma 8** (orthonormal trigonometric basis on the grid). *Let  $\psi_{\boldsymbol{\kappa}}(\mathbf{s}) = (2\pi)^{-1} \sin(2\pi\langle \boldsymbol{\kappa}, \mathbf{s} \rangle)$ ,  $\boldsymbol{\kappa} \in \mathbb{Z}^D$ . Then  $\{\psi_{\boldsymbol{\kappa}}\}_{\|\boldsymbol{\kappa}\|_{\infty} \leq m/2}$  is an orthonormal system for both the continuous and the empirical  $L_2$  norms:*

$$\langle \psi_{\boldsymbol{\kappa}}, \psi_{\boldsymbol{\kappa}'} \rangle_{L_2} = \langle \psi_{\boldsymbol{\kappa}}, \psi_{\boldsymbol{\kappa}'} \rangle_J = \delta_{\boldsymbol{\kappa}\boldsymbol{\kappa}'}$$

*Proof.* Write  $\theta(\mathbf{s}) := 2\pi\langle \boldsymbol{\kappa}, \mathbf{s} \rangle$  and note that  $\sin \theta = (e^{i\theta} - e^{-i\theta})/(2i)$ . Hence

$$\psi_{\boldsymbol{\kappa}}\psi_{\boldsymbol{\kappa}'} = \frac{2}{(2i)^2} \left\{ e^{i2\pi\langle \boldsymbol{\kappa}-\boldsymbol{\kappa}', \mathbf{s} \rangle} - e^{i2\pi\langle \boldsymbol{\kappa}+\boldsymbol{\kappa}', \mathbf{s} \rangle} - e^{-i2\pi\langle \boldsymbol{\kappa}+\boldsymbol{\kappa}', \mathbf{s} \rangle} + e^{-i2\pi\langle \boldsymbol{\kappa}-\boldsymbol{\kappa}', \mathbf{s} \rangle} \right\}.$$

Integrating each exponential over the unit cube gives 1 if its frequency vector is  $\mathbf{0}$  and 0 otherwise. Exactly one term survives when  $\boldsymbol{\kappa} = \boldsymbol{\kappa}'$ ; none survive when  $\boldsymbol{\kappa} \neq \boldsymbol{\kappa}'$ . A direct calculation implies  $\langle \psi_{\boldsymbol{\kappa}}, \psi_{\boldsymbol{\kappa}'} \rangle_{L_2} = \delta_{\boldsymbol{\kappa}\boldsymbol{\kappa}'}$ .

For the discrete inner product we use the identity

$$\sum_{j=0}^{m-1} e^{i2\pi(k-k')j/m} = \begin{cases} m, & k \equiv k' \pmod{m}, \\ 0, & \text{otherwise.} \end{cases} \quad (19)$$

Because every component of  $\boldsymbol{\kappa}$  and  $\boldsymbol{\kappa}'$  lies in  $\{-m/2, \dots, m/2\}$ , the congruence  $k_d \equiv k'_d \pmod{m}$  is equivalent to equality  $k_d = k'_d$ . Expanding the sine product as in step 1 and applying the identity (19) in each coordinate shows that  $m^{-D} \sum_{\mathbf{j}} \psi_{\boldsymbol{\kappa}}(\mathbf{s}_{\mathbf{j}})\psi_{\boldsymbol{\kappa}'}(\mathbf{s}_{\mathbf{j}}) = \delta_{\boldsymbol{\kappa}\boldsymbol{\kappa}'}$ .  $\square$

**Lemma 9** (Two well-separated Hölder functions). *Fix  $\boldsymbol{\kappa}^* := (K, 0, \dots, 0)$ ,  $K = \lceil m/4 \rceil \asymp m = J^{1/D}$ . For the amplitude  $\delta_J := c_0 J^{-1/(2+D)}$ ,  $c_0 > 0$ , define  $f_0 \equiv 0$ ,  $f_1 := \delta_J \psi_{\boldsymbol{\kappa}^*}$ . Then for  $c_0$  small enough, we have  $f_0, f_1 \in \mathcal{C}^{\nu}(B)$  for every  $\nu > 1$ ;*

$$\|f_1 - f_0\|_{L_2}^2 = c_0^2 J^{-2/(2+D)}, \quad \text{KL}(\mathbb{P}_{f_0}^J, \mathbb{P}_{f_1}^J) \leq \alpha < 1$$

*Proof.* Note that  $\psi_{\boldsymbol{\kappa}^*}$  is real analytic; its  $\alpha$ -th derivative is bounded by  $C_{\alpha} K^{|\alpha|} \leq C_{\alpha} m^{|\alpha|}$ . With  $\delta_J = c_0 m^{-(2+D)/D}$  the Hölder seminorm is bounded by  $c_0 C'_{\nu} \leq B$  for small  $c_0$ . Additionally, Lemma 8 gives  $\|f_1\|_{L_2}^2 = \delta_J^2$ . Now see that,  $\text{KL}(\mathbb{P}_{f_0}^J, \mathbb{P}_{f_1}^J) = \frac{IJ}{2\sigma^2} \delta_J^2 = \frac{Ic_0^2}{2\sigma^2} J^{D/(2+D)}$ . Since  $D/(2+D) > 0$ , choosing  $c_0^2 \leq 2\sigma^2 \alpha I^{-1} J^{-D/(2+D)}$  forces the KL to remain  $\leq \alpha$  uniformly in  $J$ .  $\square$

### Lower bound via Le Cam's two-point method

The core of this method relies on finding two functions,  $f_0$  and  $f_1$ , that are simultaneously far apart in the  $L_2$  metric but statistically close, making them difficult for any estimator to distinguish. Lemma 9 provides exactly such a pair.

Let  $\hat{f}$  be any estimator based on the data  $\mathbf{y}$  and consider the two functions  $f_0$  and  $f_1$  constructed in Lemma 9. To apply Le Cam's bound, we need two key quantities derived from that

lemma: (i) The squared  $L_2$  distance, which measures how far apart the functions are:  $\|f_1 - f_0\|_{L_2}^2 = c_0^2 J^{-2/(2+D)}$ , and (ii) the Kullback-Leibler (KL) divergence, which measures how statistically similar the data distributions are. Lemma 9 shows this can be bounded by a constant:  $\text{KL}(\mathbb{P}_{f_0}^J, \mathbb{P}_{f_1}^J) \leq \alpha < 1$ .

Using Pinsker's inequality, we convert the KL bound into a bound on the total variation distance:

$$\text{TV}(\mathbb{P}_{f_0}^J, \mathbb{P}_{f_1}^J) \leq \sqrt{\text{KL}(\mathbb{P}_{f_0}^J, \mathbb{P}_{f_1}^J)/2} \leq \sqrt{\alpha/2} < 1.$$

We now insert these components into Le Cam's two-point lower bound (Tsybakov, 2009, Lemma 2.3). The risk for any estimator over these two functions is bounded below by:

$$\sup_{f \in \{f_0, f_1\}} \mathbb{E}_f \|\hat{f} - f\|_{L_2}^2 \geq \frac{\|f_1 - f_0\|_{L_2}^2}{4} (1 - \text{TV}(\mathbb{P}_{f_0}^J, \mathbb{P}_{f_1}^J)) \geq c J^{-2/(2+D)},$$

with  $c = \frac{c_0^2}{4} (1 - \sqrt{\alpha/2}) > 0$ .

Because Lemma 9 also established that both  $f_0$  and  $f_1$  belong to the class  $\mathcal{C}^\nu(B)$ , the worst-case risk over this specific pair of functions is a valid lower bound for the minimax risk over the entire class. We therefore obtain the final result:

$$\inf_{\hat{f}} \sup_{f_0 \in \mathcal{C}^\nu(B)} \mathbb{E}_{f_0} \|\hat{f} - f_0\|_{L_2}^2 \gtrsim J^{-2/(2+D)}.$$

The proof of Theorem 2 concludes by proving the following Proposition 10, where we show that the CAR posterior mean  $\hat{f}_{\text{CAR}}$  is an admissible estimator, so its risk is bounded from below by the minimax rate just established.

**Proposition 10** (Rate-optimality of the CAR posterior mean). *Let the regression model of Assumption (A1) hold, i.e.*

$$y_j = f_0(\mathbf{s}_j) + \varepsilon_j, \quad \varepsilon_j \stackrel{i.i.d.}{\sim} \mathcal{N}(0, \sigma^2/I), \quad j = 1, \dots, J = m^D,$$

with design points on the regular grid  $\{0, \frac{1}{m}, \dots, \frac{m-1}{m}\}^D$  and  $f_0 \in \mathcal{C}^\nu(B)$  for some  $\nu > 1$ . Equip the vector  $\mathbf{f} = (f(\mathbf{s}_1), \dots, f(\mathbf{s}_J))^\top$  with the intrinsic first-order CAR prior in Assumption (A4)

$$\mathbf{f} \sim \mathcal{N}(\mathbf{0}, \tau^{-1}(\mathbf{D} - \rho \mathbf{W})^{-1}), \quad 0 < \rho < 1,$$

and let  $\hat{\mathbf{f}}_{\text{CAR}} = \mathbb{E}[\mathbf{f} \mid \mathbf{y}]$  denote the posterior mean. If the precision hyper-parameter is chosen as  $\tau \asymp m^2 \equiv J^{2/D}$ , then

$$\mathbb{E}_{f_0} \|\hat{\mathbf{f}}_{\text{CAR}} - \mathbf{f}_0\|_{L_2}^2 = \mathcal{O}(J^{-2/(2+D)}).$$

*Proof.* The proof establishes the rate of the CAR posterior mean by analyzing its Mean Squared Error (MSE) in the Fourier domain, which allows for a clear decomposition into bias and variance components.

We use the discrete orthonormal Fourier basis  $\{\psi_\kappa\}$  from Lemma 8. In this basis, the problem diagonalizes. The data  $y_j$  have Fourier coefficients  $y_\kappa = c_\kappa^0 + \varepsilon_\kappa$  where  $c_\kappa^0$  are the coefficients of the true function  $f_0$  and  $\varepsilon_\kappa$  are the coefficients of the noise. The precision of the likelihood for each coefficient is:  $\lambda_y(\kappa) = I/\sigma^2$  (constant for all  $\kappa$ ) Following the theory in Chapters 2 and 3 of Rue and Held (2005), the eigenvalues of the intrinsic first-order CAR prior precision matrix are

( $h = 1/m$ ):

$$\lambda_0(\boldsymbol{\kappa}) = \tau h^{-2} 4 \sum_{d=1}^D \sin^2(\pi \boldsymbol{\kappa}_d / m) \asymp \tau m^2 \|\boldsymbol{\kappa}\|^2 \quad (\text{for low frequencies})$$

For each frequency  $\boldsymbol{\kappa}$ , the posterior mean of the corresponding Fourier coefficient is a weighted average of the prior mean (0) and the data  $y_{\boldsymbol{\kappa}}$ :

$$\hat{c}_{\boldsymbol{\kappa}} = \frac{\lambda_y}{\lambda_y + \lambda_0(\boldsymbol{\kappa})} y_{\boldsymbol{\kappa}} = \frac{\lambda_y}{\lambda_y + \lambda_0(\boldsymbol{\kappa})} (c_{\boldsymbol{\kappa}}^0 + \varepsilon_{\boldsymbol{\kappa}})$$

The total MSE is the sum of the MSE for each coefficient. Using the fact that  $\mathbb{E}[\varepsilon_{\boldsymbol{\kappa}}] = 0$  and  $\mathbb{E}[\varepsilon_{\boldsymbol{\kappa}}^2] = \sigma^2/I = 1/\lambda_y$ , we decompose the MSE into squared bias and variance:

$$\begin{aligned} \text{MSE} &= \mathbb{E} \|\hat{f}_{\text{CAR}} - f_0\|_J^2 = \sum_{\boldsymbol{\kappa}} \mathbb{E} [(\hat{c}_{\boldsymbol{\kappa}} - c_{\boldsymbol{\kappa}}^0)^2] \\ &= \underbrace{\sum_{\boldsymbol{\kappa}} \left( \frac{\lambda_0(\boldsymbol{\kappa})}{\lambda_y + \lambda_0(\boldsymbol{\kappa})} \right)^2 |c_{\boldsymbol{\kappa}}^0|^2}_{\text{Squared Bias}} + \underbrace{\sum_{\boldsymbol{\kappa}} \frac{\lambda_y}{(\lambda_y + \lambda_0(\boldsymbol{\kappa}))^2}}_{\text{Variance}} \end{aligned}$$

The optimal rate is achieved by balancing the bias and variance terms. The CAR estimator is asymptotically equivalent to a kernel smoother of order  $m = 1$  on a regular grid (explored in [Lindgren et al. \(2011\)](#); [Kammann and Wand \(2003\)](#)). For such a smoother with an effective bandwidth  $h$ , the squared bias is dominated by smoothing error for the true function's curvature,  $\text{Bias}^2 \approx C_1 h^{2m} = C_1 h^2$ . Consequently, the variance is determined by averaging the noise over the  $J$  data points,  $\text{Var} \approx C_2/(Jh^D)$ . The total risk is minimized by choosing the bandwidth  $h$  that balances these two competing terms:

$$h^2 \approx \frac{1}{Jh^D} \implies h^{D+2} \approx \frac{1}{J} \implies h_{\text{opt}} \approx J^{-1/(D+2)}$$

Substituting this optimal bandwidth  $h_{\text{opt}}$  back into the risk expression gives the best achievable rate for this class of estimator:

$$\text{MSE} \approx (h_{\text{opt}})^2 \approx \left( J^{-1/(D+2)} \right)^2 = J^{-2/(D+2)}$$

This demonstrates that with an optimal choice of  $\tau$ , the CAR posterior mean achieves the minimax rate of  $\mathcal{O}(J^{-2/(D+2)})$ . Since Theorem 2 gives the *same* rate as a minimax lower bound, the CAR posterior mean is minimax-optimal on  $C^\nu(B)$ .  $\square$